Monomolecular Multimodal Fluorescence-Radioisotope Imaging Agents

Zongren Zhang, Kexian Liang, Sharon Bloch, Mikhail Berezin, and Samuel Achilefu*

Department of Radiology, Washington University, St. Louis, Missouri 63110. Received May 5, 2005; Revised Manuscript Received August 8, 2005

Diagnosis of diseases by different imaging methods can provide complementary information about the functional status of diseased tissues or organs. To overcome the current difficulties in coregistering images from different imaging modalities with a high degree of accuracy, we prepared near-infrared (NIR) monomolecular multimodal imaging agents (MOMIAs) consisting of a heptamethine carbocyanine and ^{111}In−DOTA chelate that served as antennae for optical and scintigraphic imaging, respectively. Their spectral properties clearly show that coordination of indium to MOMIA increased the fluorescence intensity of the compounds. The MOMIAs are exceptionally stable in biological media and serum up to 24 h at 37 °C. Biodistribution of the compounds in mice obtained by fluorescence photon and γ-counts demonstrated a similar distribution trend of the molecular probe in different tissues, suggesting that the detected fluorescence and γ-emissions emanated from the same source (MOMIA). At 24 h postinjection, the MOMIAs were excreted by the renal and hepatobiliary systems and the blood level of a representative MOMIA was very low, thereby reducing background noise caused by circulating molecular probes. These findings demonstrate the feasibility of preparing single molecules with the capacity to emit discernible and diagnostic fluorescent and γ-radiations for optical and nuclear imaging of living organisms.

INTRODUCTION

Coregistration of tissue with different imaging modalities can furnish unique and complementary information that improves the accuracy of disease diagnosis and enhances patient management (*1*, *2*). For example, coregistration of tumors with magnetic resonance imaging (MRI) and positron emission tomography provides anatomical and functional information, which can be used to visualize metastatic foci and localize its exact position (*3*). These possibilities have led to the development of multimodal imaging instruments for clinical and preclinical applications.

Optical imaging is an emerging method that can benefit from a multimodal imaging strategy. The method is highly sensitive, with the capability of detecting minute amounts of light emitting materials in heterogeneous mediums (*4*, *5*). In addition, optical imaging also uses low energy radiation in the visible and infrared regions of the electromagnetic spectrum of light to assess biological processes in tissues. The distribution of chromophores within a few micrometers from the light source and detector systems can be localized with high resolution, thereby permitting the differentiation of normal from pathologic tissues (*6*−*8*). However, the ability to detect diagnostic chromophores and the image resolution obtained by optical methods degrade rapidly as the distance between source−detector pair and the target tissue volume progressively increases beyond several centimeters. This poor resolution is caused by the intrinsic absorption and scattering of light by tissue. Therefore, for noninvasive deep tissue imaging, optical methods would benefit from a multimodal strategy that can complement this weakness. Additionally, a multimodal approach that combines optical with one of the established imaging methods could accelerate its acceptance in clinical settings.

Recently, Ntziachristos et al. (*9*) coregistered indocyanine green (ICG)-enhanced optical images of breast cancer patients with DTPA−Gd-enhanced MRI. The results demonstrate that diffuse optical tomography can adequately localize and quantify exogenous optical contrast agents in breast cancers. Typical of most current multimodal imaging procedures, the investigators administered two different contrast agents to patients: a paramagnetic gadolinium DTPA chelate for MRI and ICG for optical imaging. Expectedly, the pharmacokinetics of both probes were very different and the potential toxic effects of each component can be additive. Understandably, a major problem with developing a single molecular entity that can produce detectable signals for each imaging method derives from differences in the sensitivities of each modality. For example, the design of a monomolecular Gd-based MRI−optical monomolecular multimodal imaging agent (MOMIA) must incorporate multiple Gd chelates per dye moiety to compensate for the relatively low sensitivity of the MRI method. Some common strategies employed to compensate for the large differences in local tissue sensitivities of different imaging systems require the use of large biomolecules, polymeric materials, liposomes, micelles, or nanoparticles (*10*−*13*). However, the inherent problems with large molecules, including low diffusion rate into diseased tissue, rapid uptake by the liver, and the potential to elicit adverse immune reactions, limit their utility as contrast agents for in vivo imaging studies (*14*). Recent approaches include the use of smaller molecular constructs to obtain multimodal agents for MRI and optical imaging studies (*15*).

The sensitivities of fluorescence and radionuclear

* To whom correspondence should be addressed. Tel: 314-362-8599. Fax: 314-747-5191. E-mail: achilefus@mir.wustl.edu.

10.1021/bc050136s CCC: $30.25
Published on Web 08/25/2005

methods are comparable, which enable the incorporation of antennae for both methods into a relatively small molecular mass (<6 kDa) single molecule in a 1:1 signaling ratio. This optical−radionuclear molecular construct would allow the use of a short-lived radioisotope component of the MOMIA to localize diseases in deep tissue without the depth limitation of optical methods. After mapping the region of interest, longitudinal monitoring of the diseased tissue can be conducted by optical methods outside radioactivity restricted areas. Optical imaging in the near-infrared (NIR) region minimizes light attenuation by endogenous chromophores and facilitates deep tissue imaging. Accordingly, we report the synthesis of NIR light emitting dye−DOTA conjugates linked by alkyl or peptidyl units. We further assessed their spectral properties and biodistribution in mice. The fluorescence and γ-counts of the MOMIAs in different tissues were similar and demonstrate the feasibility of developing these molecular constructs for multimodal imaging by tandem optical and radionuclear methods.

MATERIALS AND METHODS

General. All solvents and chemicals were reagent grade and used without further purification. *N,N*-Diisopropylcarbodiimide (DIC) and glutaconaldehyde dianilide monohydrochloride were purchased from Lancaster Synthesis (Windham, NH). Dichloromethane (DCM), *N*,*N*-dimethylformamide (DMF), MeOH, and MeCN were from purchased from Fisher Scientific (Pittsburgh, PA). Fluorenylmethyl amino acids (Fmoc) and trifluoroacetic acid (TFA) were purchased from, respectively, AnaSpec Inc. (San Jose, CA) and Advanced ChemTech (Louisville, KY). Other commercial chemicals were purchased from Sigma-Aldrich (St. Louis, MO). Mass spectral analyses were performed on a Waters ZQ 4000 positive electrospray at a cone voltage of 67 V. All of the compounds including the intermediates and final products were fully identified by mass spectrometry/electrospray ionization high-performance liquid chromatography (MS/ESI HPLC) analyses performed on a Vydac C-18 polymeric reverse phase column (218TP, 5 μm, 300 Å, 4.6 mm × 250 mm) at a flow rate of 1.0 mL/min. Semipreparative HPLC was performed on a Vydac C-18 polymeric reverse phase column (218TP, 10 μm, 300 Å, 22 mm × 250 mm) at 9.5 mL/min. HPLC solvents consist of water containing 0.1% TFA (solvent A) and MeCN containing 0.1% TFA (solvent B). The elution protocol for analytical HPLC started with 90% A for 1 min, followed by a linear gradient to 30% A over 20 min, held at 30% A for 5 min, continued to 10% A for 5 min, and finally returned to 90% A over 2 min. The elution profiles of MOMIAs were monitored by UV absorbance at 254 and 214 nm. Absorbance spectra were measured on a Beckman Coulter DU 640 UV−visible spectrophotometer. Fluorescence spectra were recorded on a Fluorolog-3 spectrofluorometer (Horiba Jobin Yvon, Inc., Edison, NJ). Stock solutions (1.0 mM) of the dye and its conjugates were prepared by dissolving each sample in DMSO. UV−vis and fluorescence measurements were carried out by sequentially adding 0.5−2.0 μL aliquots of the stock solutions via a micropipet into 3 mL of 20% aqueous DMSO solution or other solvents in a quartz cuvette. The mixtures were stirred briefly for equilibration prior to data acquisition.

Synthesis of Cypate (1). Ac_2O (226 μL, 2.4 mmol) in DCM (1 mL) was added slowly to a stirred solution of glutaconic aldehyde dianilide hydrochloride (0.6 g, 2 mmol) and diisopropyl ethylamine (DIEA, 700 μL, 4 mmol) in DCM (4 mL). The solution was added to a warm (50 °C), stirred MeCN (10 mL) solution of NaOAc (0.8 g, 9.5 mmol) and 1-hydroxycarbonylethyl-2,3,3-trimethylbenzoindoleninium bromide (2.0 g, 5.5 mmol), which was prepared as described previously (*16*). The mixture was stirred for 30 min at 50 °C to give noticeable precipitates. Additional precipitates were obtained by adding ether to the reaction mixture. The solid was filtered and washed sequentially with ether, MeCN, ether, and water (1% TFA) to give 1.06 g (85%) of **1** as a red glistening solid. MS/ESI: 625 [M^+].

Synthesis of Tri-*t*-butyl DOTA (2). Benzyl bromoacetate (4.0 g, 17 mmol) in MeCN (80 mL) was added dropwise (3.5 h) to an ice-cooled mixture of K_2CO_3 (6.5 g, 47 mmol) and 1,4,7,10-tetraazacyclododecane tetrahydrochloride (5.0 g, 15.7 mmol) in MeCN (50 mL). The mixture was stirred for 30 min at 0 °C. K_2CO_3 (3.5 g, 25 mmol) was added as a solid, followed by dropwise (1 h) addition of *tert*-butyl bromoacetate (12.3 g, 62.8 mmol) in MeCN (80 mL). The resulting mixture was stirred at 0 °C overnight, and the solid was filtered. After the solid was further washed with MeCN/MeOH, the collected filtrates were combined and acidified with TFA to pH 5. The precipitate obtained after acidification was filtered and concentrated on a rotary evaporator. The solid residue was washed with ether and dried to give 9.3 g of a white powder. HPLC and MS studies indicated that powder consisted of 60% benzyl tri-*tert*-butyl DOTA and 40% tetra-*tert*-butyl DOTA. Because the tetra-*tert*-butyl byproduct is not reactive, the product mixture can be used in subsequent reactions without prior purification. MS/ESI: 663 [$M + H^+$], 701 [$M + K^+$].

Hydrogen was bubbled through a mixture of the solid (3 g) and Pd/C (10 wt %, 300 mg) in THF (180 mL)/MeOH (180 mL) at atmospheric pressure for 15 h. The Pd/C catalyst was removed by filtration, and the solvent was removed on a rotary evaporator to give crude solid product. The solid was further purified by recrystallization in acetone/*t*-BuOMe/hexanes system to give **2** (1.8 g) as a white solid. MS/ESI: 573 [$M + H^+$].

Synthesis of Tri-*t*-butyl DOTA−Hexanediamine−Cypate (4a). A mixture of tri-*tert*-butyl DOTA (349.2 μmol, 200 mg), 2-(1*H*-benzotriazol-1-yl)-1,1,3,3-tetramethyluronium hexafluorophosphate (HBTU, 134 mg, 358 μmol), and *N*-hydroxybenzotriazole (HOBt, 50 mg, 326 μmol) in DMF/DCM (50:50 vol %, 7 mL) was shaken for 5 min. DIEA (92 μL, 523.8 μmol) was then added, and the mixture was shaken again for 10 min. 1,6-Hexanediamine (419.04 μmol, 49 mg) was added as a solid, and the mixture was shaken for 2 h before cypate (327 mg, 523.8 μmol), activated similarly, was added. The resulting mixture was shaken for 4 h. It was neutralized with dilute HCl (0.1 M). DCM was removed on a rotary evaporator, and the concentrated solution was treated with ether to precipitate the product, which was further washed sequentially with water, ether, and ethyl acetate. Pure product was isolated by semipreparative HPLC to give 40 mg of **4a**. MS/ESI: 1277 [M^+].

Synthesis of DOTA−Hexanediamine−Cypate (4). Tri-*tert*-butyl DOTA−hexanediamine−cypate (**4a**, 10.5 mg, 8.2 μmol) in TFA (2 mL) was stirred for 2 h at room temperature. TFA was removed, and the resulting green solid was washed with ether and separated by semipreparative HPLC to give 1.3 mg (1.17 μmol, 15% yield) of **4** as a green solid. MS/ESI: 1109 [M^+].

Synthesis of α−DOTA−Lys(ϵ-Cypate)−OH (5). Fmoc−Lys(Dde)−OH (655 mg, 1.23 mmol) in DCM (5 mL) and DMF (0.2 mL) was cooled by ice bath, and DIC (615 μmol, 96 μL) was added. The mixture was stirred at 0 °C for 20 min. DCM was removed on a rotary evaporator, and the residue was dissolved in DMF (5 mL).

The solution was transferred to a mixture of 4-(dimethylamino)pyridine (2.5 mg, 20.5 μmol) and Wang resin (100−200 mesh, 0.82 mmol/g, 250 mg, 205 μmol) preswelled in DMF. The mixture was shaken for 3 h, followed by filtration and sequential washing with DMF−MeOH−DMF−DCM−DMF. Fmoc was removed with 20% piperidine in DMSO and tri-*tert*-butyl DOTA (352 mg, 615 μmol), activated with HOBt (94 mg, 615 μmol)/HBTU (233 mg, 615 μmol)/DIEA (1.23 mmol. 214 μL), was conjugated to the α-amino group of lysine for 20 h. The Dde group was removed with 2% hydrazine in DMF and cypate (307 mg, 492 μmol) in DMF (2 mL)/DCM (2 mL), preactivated with HBTU (187 mg, 492 μmol) and HOBt (75 mg, 492 μmol), and DIEA (656 μmol, 114 μL) was added to the resin. The mixture was shaken for 5 h, filtered, and washed sequentially with DMF−DCM−DMF−DCM−DMF solvent system. The crude product was cleaved from the resin by shaking in TFA (5 mL) for 3 h. The product was purified by semipreparative HPLC to give 40 mg of the compound as a green solid. MS/ESI: 1139 $[M^+]$.

Synthesis of DOTA−Gly−Ser−Gly−Lys(ε-Cypate)−Ahx[1]−NH_2 (6). The peptides were prepared with ACT APEX 396 peptide synthesizer by standard Fmoc protocol (*17*), as described previously (*18*, *19*). Briefly, starting with a Rink amide resin, the Fmoc−Ahx−OH (75 μmol) was activated with a mixture of the coupling reagents HOBt (75 μmol) and HBTU (75 μmol) in the presence of DIEA (150 μmol). Deprotection of the Fmoc protecting group was accomplished with 20% piperidine in DMF. The tri-*tert*-butyl DOTA (75 μmol) was automatically coupled to the N-terminal amino group. The orthogonal protecting lysine group 2-(4,4-dimethyl-2.6-dioxycyclohexylidene)ethyl (Dde) was selectively removed with 2% hydrazine in DMF before adding the NIR probe, cypate. Simultaneous removal of side chain protecting groups and cleavage of the product from solid support were accomplished with a cleavage mixture of 95% TFA and 5% water. After lyophilization, the crude product was obtained as a green powder and purified by semipreparative HPLC to give **6** (6.5 mg, 18% yield). MS/ESI: 1453 $[MH]^+$, 727 $[M + 2H]^{2+}$.

Synthesis of Nonradioactive ^{115}In−MOMIAs (7 and 8). The labeling of compound **6** to give **8** is typical of the procedure used to successfully label MOMIAs with indium. Two drops of absolute ethanol were added to 2.3 mg (1.5 μmol) of compound **6** to form slurry. To this slurry was added 1 mL of a NaOAc−sodium ascorbate buffer (50 mM of NaOAc and 25 mM of sodium ascorbate). A solution of $InCl_3$ in 0.1 M HCl (1 mL, 1.1 mg, 4.74 μmol) was added to the reaction mixture to obtain a solution of pH 4.9. The solution was heated at 80 °C for 1 h, and the mixture was allowed to cool to room temperature. The solution retained its green color, and the product was purified by semipreparative HPLC using MeCN/H_2O gradient elution protocol (see General section above) to give 1.2 mg (0.77 μmol, 49% yield) of **6**. MS/ESI: 1564 $[M]^+$.

Similarly, compound **7** was prepared by adding $InCl_3$ (18.5 mg, 16 μmol) to a MeCN/water solution of **4** (15 mg, 13 μmol). The mixture was purified by semipreparative HPLC to obtain 2 mg (13%) of **7**. MS/ESI: 1221 $[M]^+$.

Radiolabeling of MOMIAs with ^{111}In (9). $^{111}InCl_3$ was purchased from Mallinckrodt, Inc. Compound **6** was radiolabeled by incubating 5.0 μg of it with 50 μCi of ^{111}In in a 25 mM NaOAc and 12.5 mM sodium ascorbate buffer. The pH was adjusted to 4.9 with 0.1 M HCl to give a total volume of 55 μL. The mixture was heated at 80 °C for 30 min. An equal volume of PBS containing 5% EtOH was added, and the solution was allowed to cool to room temperature. Visual inspection shows that it retained its green coloration after 24 h. Radio-TLC showed that the labeling was successful. An aliquot was placed in a tube and imaged with a Kodak Multistation Imager.

Stability of ^{115}In−DOTA−Gly−Ser−Gly−Lys(ε-Cypate)−Ahx−NH_2 (8). The stability of the representative compound was conducted using HPLC (Waters, Co.) by monitoring the signal intensity at 700 nm from a dual UV-vis absorbance detector. The 700 nm wavelength was chosen to avoid otherwise strong overlapping of signals between the serum and the compound **8** at lower wavelengths. HPLC analyses were conducted using Vydac C-18 polymeric reverse phase column (218TP, 5 μm, 300 Å, 4.6 mm × 100 mm) with water/MeCN−0.1% TFA mobile phase with a gradient from 10 to 95% MeCN in water in 14 min.

Approximately 0.2 mg of the lyophilized complex was dissolved first in 20 μL of DMSO and diluted with 80 μL of water. The solution was split into two vials: 60 μL was added into 940 μL of human serum in a 2 mL vial, and 30 μL was diluted with 470 μL of water (MQ). The vial with serum was capped and placed in an incubator at 37 °C. Aliquots of 60 μL were analyzed without dilution at different time points. The vial without serum was used as a reference standard. In addition, a standard serum solution was prepared by mixing 12 μL of DMSO, 48 μL of water (MQ), and 940 μL of human serum.

Biodistribution of MOMIAs by Fluorescence Method. All in vivo studies were performed in compliance with the Washington University Animal Study Committee's requirements for the care and use of laboratory animals in research. Nude mice were anesthetized with xylazine/ketamine cocktail via intraperitoneal injection. The samples were dissolved in 20% aqueous DMSO, and animals were injected via the lateral tail vein with doses of 0.3 μmol/kg body weight in a volume of 100 μL for each mouse. We used a noninvasive in vivo continuous wave fluorescence imaging apparatus to visualize the distribution and preferential tissue uptake of the MOMIAs.

Light from two laser diodes of nominal wavelength 780 nm and nominal power of 50 mW was launched into a fiber optic bundle. We used two laser diodes to produce as much uniform illumination of the whole animal or organ parts as possible. A defocusing lens in position after the bundle expanded the beam such that the whole mouse was illuminated. A Photometrics CCD camera (16 bit, 1024 × 1024 pixels, back illuminated, thermoelectric Peltier cooled with forced air) was used to capture the emitted photons. An interference filter (830 nm) was mounted in front of the CCD camera input lens such that only emitted fluorescent light from the contrast agent was imaged. Real-time acquisition, display, and data processing software (WinView/32) were used to obtain the optical imaging data.

At 24 h postinjection of the probe, the mice were euthanized and some organ parts were excised and rinsed with water. The tissues were placed under the CCD camera and the fluorescence emission from each organ was measured after excitation with the 780 nm laser sources. Tissue parts, instead of whole organs, were used to minimize problems associated with depth-dependent nonlinear fluorescence emission. A statistical program in the WinView package was used to estimate the mean fluorescence intensity per organ part.

[1] 6-Amino hexanoic acid.

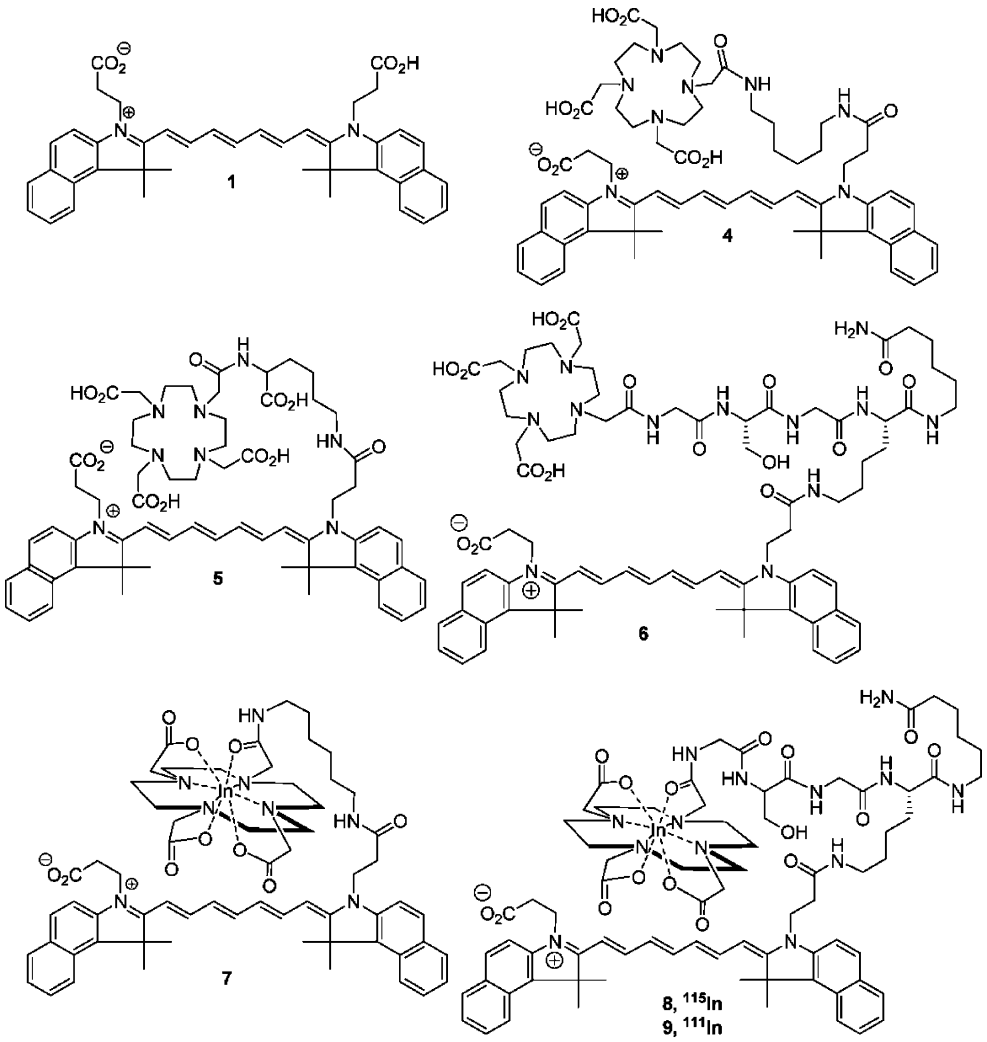

Figure 1. Structures of cypate, DOTA−cypate, and In−DOTA−cypate derivatives.

Scheme 1. Synthesis of DOTA−Ahx−Cypate MOMIA by Solution Method

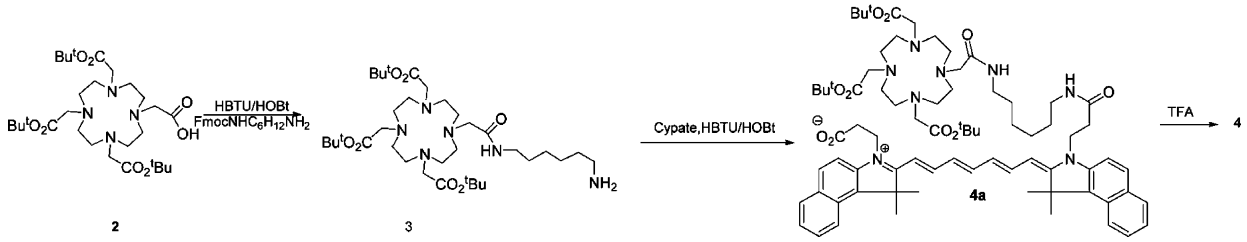

Biodistribution of MOMIAs by γ-Counts Method. The mice were anesthetized as described above and injected with 10 μCi (100 μL) of ^{111}In labeled **9** via the lateral tail vein. Mice were imaged 1, 4, and 24 h postinjection with a Kodak Multistation Imager. At 24 h postinjection, we sacrificed the animals and weighed the organ parts and the activity/g organ was determined with a Packard Cobra II γ-counter.

RESULTS AND DISCUSSION

The primary focus of this study was to develop novel optical−radionuclear MOMIAs that could provide complementary diagnostic information, minimize patient's exposure to ionizing radiation, simplify image reconstruction for optical diffusion tomography, and provide a means to monitor continuously the status of pathologic conditions by optical methods after the decay of a short-lived radioactive component. The use of NIR fluorescent dye for the optical signal allows for deep tissue imaging because absorption of light by tissue in this region is low, thereby allowing NIR light to penetrate several centimeters (*20*, *21*). We used ^{115}In isotope for nonradionuclear related studies to avoid contaminating routine laboratory instruments with radioactivity.

Synthesis. The MOMIAs (Figure 1) were synthesized by either solid phase or solution methods, based on the target compounds prepared.

Synthesis of MOMIAs by Solution Method. The procedure for the synthesis of **4** is summarized in Scheme 1. Both DOTA and cypate possess multiple carboxylic acid groups, and linkage of the two components via amide bonds with a diamino group would result in an intractable mixture of products. To improve reaction selectivity, we first reacted an orthogonally protected tri-*tert*-butyl DOTA (**2**) with a mono-Fmoc−1,6-hexyldiamine, followed by purification of the crude product on a silica gel column.

Scheme 2. Solid Phase Approach to the Synthesis of MOMIAs

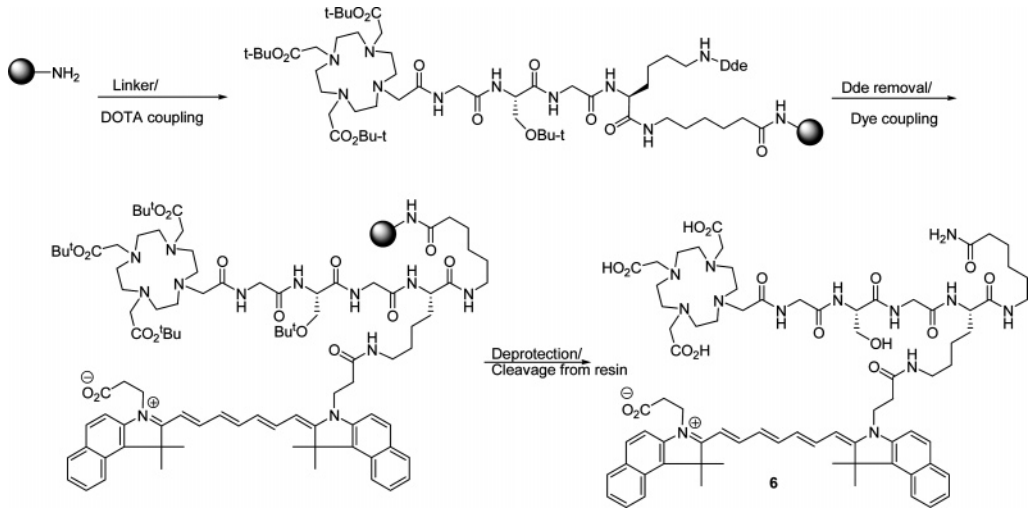

It turned out that the Fmoc derivative was unstable during column purification, and compound **3** was isolated as the major product. This protocol, therefore, results in the direct synthesis of monoamino derivative of tri-*tert*-butyl DOTA. Through a careful control of the reaction conditions, compound **3** reacted with only one of the two carboxylic acid groups of cypate to afford **4a**. Subsequent treatment of **4a** with TFA gave the desired compound **4** in good yield. However, the intermediate Fmoc-protected DOTA−amine was unstable under ambient conditions and its purification was tedious. Consequently, we evaluated the preparation of MOMIAs by solid phase method (*17*, *18*).

Synthesis of MOMIAs by Solid Phase Method. Syntheses of MOMIAs **5** and **6** were conducted on solid support as summarized in Scheme 2 for the synthesis of **6**. The use of orthogonally protected amino acid strategy enabled us to selectively couple DOTA and cypate without interference from each other. Cleavage of the product from resin using TFA and subsequent workup afforded the desired compounds.

Labeling MOMIAs with Indium. The stability of the metal complexes of MOMIAs is a critical criterion for the use of DOTA−cypate conjugates for multimodal imaging. For this reason, we labeled the MOMIAs with both radioactive (^{111}In) and nonradioactive (^{115}In) isotopes. The radiolabeled analogues were used to evaluate the stability of the chelates in buffers and to perform the in vivo imaging studies. We used the nonradioactive chelate to monitor the HPLC stability of MOMIAs in serum by fluorescence assay and the effects of the metal complex on the fluorescence intensity relative to the unlabeled MOMIAs. The compounds were stable under HPLC purification conditions. Interestingly, the chelated and nonchelated MOMIAs had similar retention times when they were coinjected in the column. This suggests that the chelation of MOMIAs with indium has little effect on the hydrophilicity of the compounds. Mass spectral analysis of the purified MOMIA showed that the metal chelation was successful.

Spectral Properties of MOMIAs. An important consideration in designing MOMIAs is to ensure that the fluorescence emission of the compounds is not quenched after metal chelation. Consequently, we compared the spectral properties of the labeled and nonlabeled MOMIAs. The spectra of **6** and its In−DOTA complex **8** are typical of the indium-labeled MOMIAs. Both compounds are soluble in water, making it possible to prepare metal

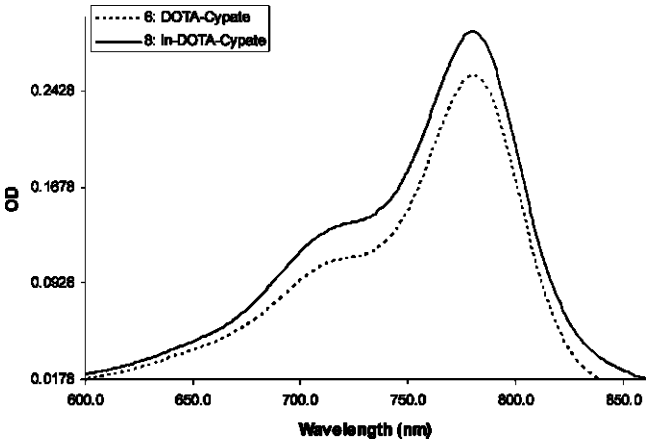

Figure 2. Absorption spectral properties of compounds **6** and **8** in water. The optical density and molar absorptivity of In chelate **8** are higher than those of the nonchelate analogue **6** at 1.8 μM.

complexes and study their spectral properties in aqueous medium. Equimolar concentrations (1.8 μM) of pure (>99% HPLC/MS purity) chelated and nonchelated compounds were prepared in deionized water. The absorption spectra of the compounds are shown in Figure 2. Interestingly, coordination of the metal increased the absorbance of **8** as compared with the nonchelated **6**. This spectral observation was confirmed by analysis of the molar absorptivity of both compounds, which showed a 16% increase in the molar absorptivity of **8** (ϵ 1.67 $\times$ 10^5 M^{-1} cm^{-1}) relative to the nonchelated **6** (ϵ 1.43 $\times$ 10^5 M^{-1} cm^{-1}).

Similarly, we evaluated the fluorescence emission of the compounds at an equimolar concentration of 1.8 μM at 760 and 780 nm excitation wavelengths. The full emission spectra at 760 nm excitation are shown in Figure 3, and the changes in their relative fluorescence intensity at 805 nm emission wavelength are shown in Table 1. This observation is consistent with the established effects of metals on the fluorescence properties of dyes (*22*, *23*). Particularly, this study suggests that radioisotopes of trivalent metals such as indium could play a dual role of providing γ-emissions for radionuclear imaging and augmenting the fluorescent intensity of molecular probes that would increase the sensitivity of detecting their distribution in tissues. Another interesting implication of the observed increase in fluorescence intensity after chelation of indium is that the changes

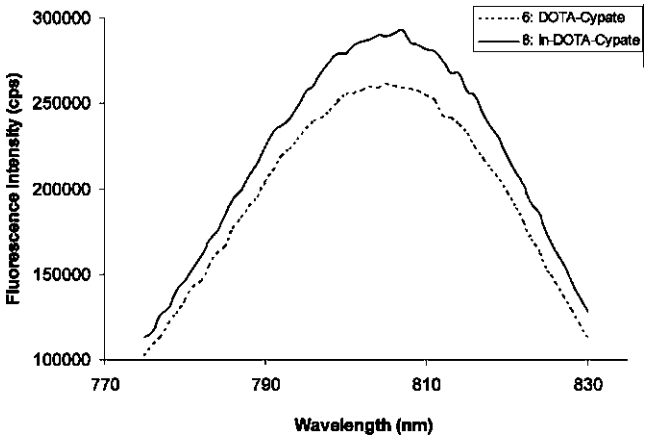

Figure 3. Fluorescence spectra of **6** (DOTA−cypate) and **8** (In−DOTA−cypate complex) in water at 760 nm excitation.

Table 1. Fluorescence Intensities of 6 and 8 at 760 and 780 nm Excitation Monitored at 805 nm Emission

excitation wavelength (nm)	fluorescence intensity of **6** at 805 nm/10^5 (cps)[a]	fluorescence intensity of **8** at 805 nm/10^5 (cps)	increase in fluorescence intensity (%)
760	2.60	2.93	13
780	2.29	2.42	6

[a] cps, photon counts per second.

are wavelength-dependent (Table 1). Conceptually, such wavelength dependency could be used for ratiometric imaging at two or more different wavelengths to increase the specificity of optical imaging methods.

Stability in Biological Media. The stability study of **8** was conducted by monitoring the signals from a dual UV absorbance detector at 254 and 700 nm on an HPLC system. At 254 nm, the signals from serum and **8** (retention time 8.4 min) strongly overlapped with prevailing signals from serum proteins. At 700 nm, the overlap was much weaker and the absorbance from **8** was dominant. Figure 4a,b shows the HPLC spectra of **8** and serum, which were also used as reference standards. Degradation was typically manifested by a gradual increase of one or more peaks as a function of time.

The indium complex showed remarkable hydrolytic stability in human serum. Taken within the first 2.5 h, the chromatograms were practically indistinguishable (Figure 5). Even after 48 h, no significant variations were observed in indium complex signal intensity (Figure 6), although some changes are noticeable between 1 and 6 min of the retention time.

Radio-TLC analyses (for radioactive indium MOMIA) showed that the compounds are stable in buffers up to 4 h postpreparation of the materials. The biodistribution studies did not show uptake of the MOMIAs in bone tissues, which is a useful index of chelate stability in vivo. Therefore, the MOMIAs are stable in serum and biological buffers.

The ability to monitor stability profile of the probes at 700 nm is advantageous because only the NIR probes absorb significantly in this spectral region, thereby eliminating the need to isolate the compounds before analysis. The data are reproducible with high precision because specific volumes from the same sample can be injected and the sample absorbance at the onset of the experiment acts as reference throughout the study.

Biodistribution of MOMIAs in Mice. *Optical Method.* Injection of MOMIAs into the lateral veins of mice and monitoring the distribution of the probe as a function of time showed that at 24 h postinjection, the molecular

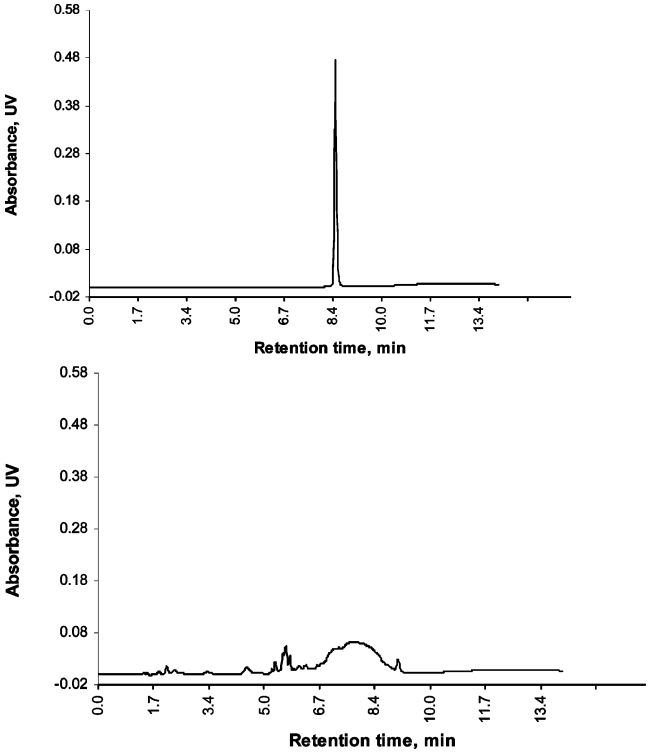

Figure 4. (a) HPLC spectrum of a standard:indium complex in DMSO/water; (b) HPLC spectrum of a standard:human serum with DMSO/water.

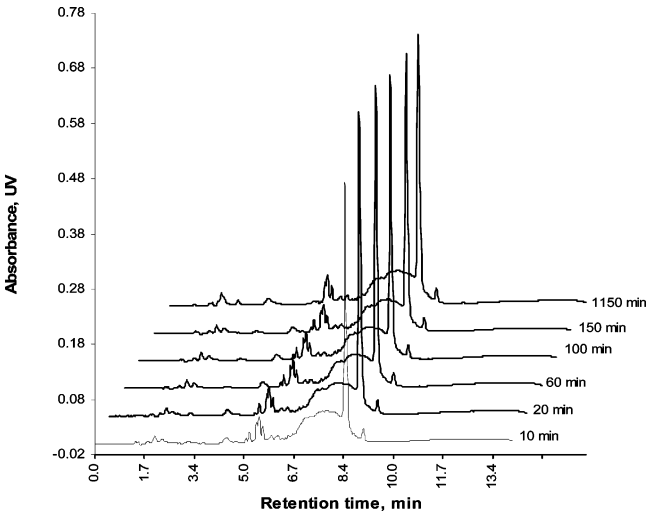

Figure 5. HPLC spectra of indium complex **8** incubating in human serum at 37 °C at different time intervals shows outstanding hydrolytic stability of the complex. Chromatograms were shifted in both *x*- and *y*-axes for clarity.

probe was retained primarily in the liver and kidneys (Figure 7). The relative fluorescence intensity was obtained as the average intensity in the organs of interest. Expectedly, the more hydrophobic **4** was retained in many normal tissues as compared with **6**, which cleared from all organs at 24 h postinjection, except the liver and kidneys. For practical purposes, rapid clearance of molecular probes from nontarget tissues is highly desirable during imaging studies to minimize background signals from these probes. As a result, detection of high fluorescence in nonexcretory organs would provide important diagnostic information within a short period postinjection of the probe. This result suggests that compound **6** is suitable for designing target specific molecular probes for multimodal imaging.

Table 2. Fluorescence Intensity[a] Distribution of Compounds 4 and 6 in Mice at 24 h Postinjection

	organ/blood ratios (of relative fluorescence) at 24 h postinjection							
compd	liver	kidney	spleen	pancreas	muscle	adrenal	heart	brain
4	11.2 ±1.2	6.6 ±1.1	3.4 ±1.1	2.6 ±1.1	1.5 ±1.0	3.0 ±1.1	NA	NA
6	78.8 ±10.3	38.1 ±4.0	1.9 ±0.9	3.8 ±1.1	2.4 ±1.1	4.5 ±1.3	3.3 ±1.1	1.7 ±1.0

[a] Fluorescence intensity was initially normalized relative to blood.

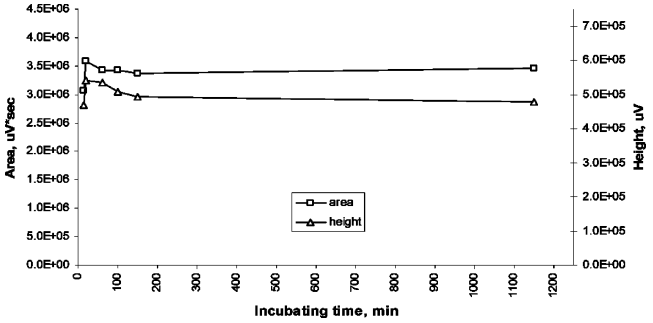

Figure 6. Quantitative results obtained by integration of area and height measurements at 8.3 min retention time shows the stability of indium complex **8**. The trace was obtained from a single test sample.

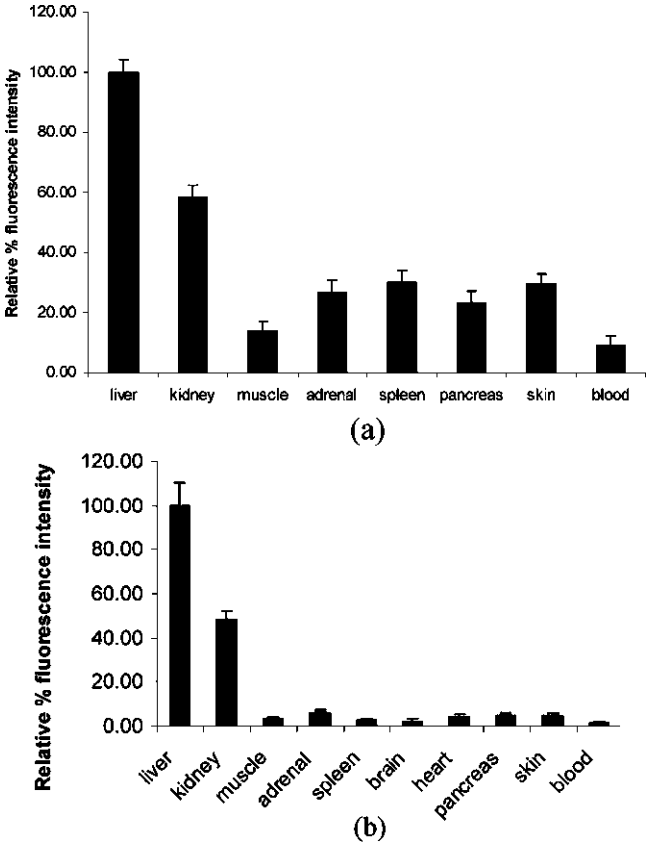

Figure 7. Distribution of (a) **4** and (b) **6** in nude mice at 24 h postinjection. Fluorescence intensity normalized to blood.

The ratio of the fluorescence intensity at 24 h relative to blood is shown in Table 2, indicating that most of the probe cleared from the body via urine (injected dose is 0.3 μmol/kg body weight of mouse; collected urine samples fluoresced). Interestingly, the fluorescence intensity of compound **6** in the brain was nearly twice relative to blood. Although this intensity is low as compared with the liver, it raises the possibility of optimizing compound **6** for brain imaging. Designing compounds that can cross the blood−brain barrier remains a challenge for imaging the brain with nonradionuclide imaging agents because

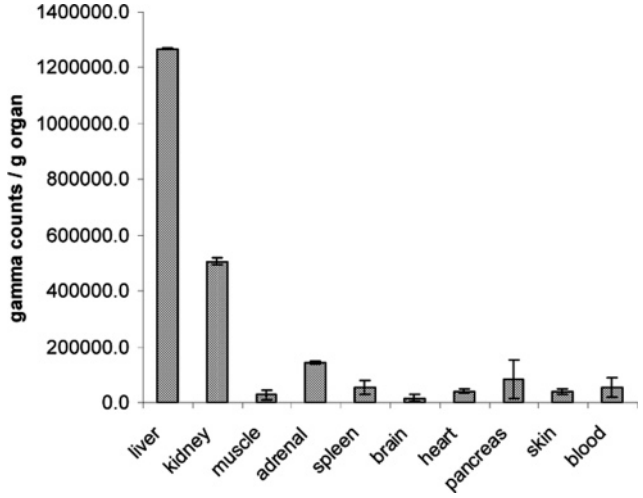

Figure 8. Biodistribution of **9** obtained by γ-counting method at 24 h postinjection.

Table 3. Distribution of 9 in Mice at 24 h Postinjection

	organ/blood ratios of γ-counts/ g organ at 24 h postinjection							
compd	liver	kidney	spleen	pancreas	muscle	adrenal	heart	brain
9	40.3	15.8	2.3	1.2	1.3	4.6	1.5	0.8

of the typical low molecular weight and nonionic molecule requirements. However, a closer look at the structure of **6** shows that the molecule can adopt a neutral configuration where all of the four carboxylic acid groups are neutralized by the tertiary amino groups. Subsequent transport across the blood−brain barrier could be mediated by phosphorylation of the serine hydroxyl group. Further studies will be needed to explore this possibility.

Radionuclear Method. γ-Emitters are routinely used for radionuclear imaging by planar or 3D SPECT techniques (*24*, *25*). Our interest in γ-scintigraphy is due to its simplicity and high sensitivity. Unlike MR and CT imaging methods that require local tissue concentration of 10^{-4} (gadolinium or manganese) and 10^{-2} M (iodine or barium) of contrast agents for diagnostic imaging, γ-scintigraphy detects about 10^{-10} M of radiopharmaceuticals (^{111}In or ^{99m}Tc) in tissues (*1*, *10*). This sensitivity is improved in SPECT, which also has a higher anatomical resolution. The detection sensitivity of optical methods falls with the range of γ-scintigraphy, depending on the optical technique employed.

The radioactive indium was prepared as described in the Materials and Methods section. We injected 10 μCi of the ^{111}In−MOMIA (**9**) and conducted the scintigraphy on a Kodak multistation imager at 1, 4, and 24 h postinjection. At 24 h postinjection, we sacrificed the animals and weighed the organ parts and the activity was determined with a γ-counter. Figure 8 shows the biodistribution of the γ-counts normalized per gram organ, and Table 3 depicts the ratios of the γ-counts normalized to 1 g of blood. The biodistribution trend observed is similar to that obtained by the fluorescence intensity method, as summarized in Figure 9. The reason for the observed slight differences in the signal intensities

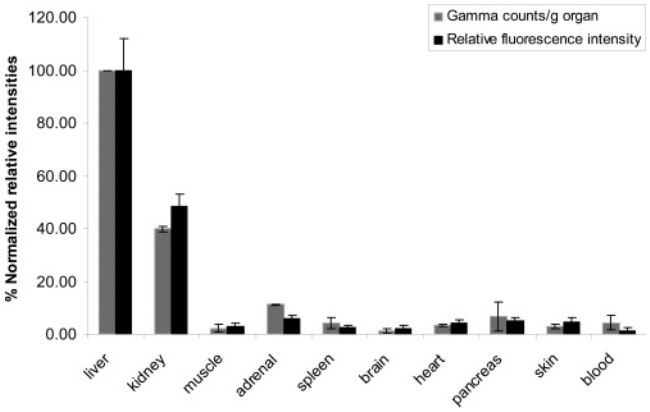

Figure 9. Comparative distribution of **8** and **9** obtained by γ- and fluorescence emission methods, respectively, at 24 postinjection of the molecular probes.

by both methods in some organs such as the kigneys and adrenal glands is probably due to interanimal biological variations.

CONCLUSION

We successfully prepared MOMIAs in good yields and successfully labeled them with radioactive and nonradioactive indium. As shown above, indium chelates of MOMIAs either retained or increased their fluorescence emission relative to the nonchelated MOMIAs. We also showed that the chelated and nonchelated MOMIAs are exceptionally stable in serum up to 48 h postincubation at 37 °C. The biodistribution studies by optical and radionuclear methods showed similar trends, indicating that both fluorescence and γ-emissions emanated from the same source. These findings demonstrate the feasibility of using MOMIA strategy to image tissues by combined optical and nuclear methods.

ACKNOWLEDGMENT

This study was supported by the National Institutes of Health (R33 CA100972).

LITERATURE CITED

(1) Allport, J. R., and Weissleder, R. (2001) In vivo imaging of gene and cell therapies. *Exp. Hematol. 29*, 1237−1246.
(2) Sabbah, P., Foehrenbach, H., Dutertre, G., Nioche, C., and DeDreuille, O., et al. (2002) Multimodal anatomic, functional, and metabolic brain imaging for tumor resection. *Clin. Imaging 26*, 6−12.
(3) Rubello, D., Casara, D., Fiore, D., Muzzio, P., and Zonzin, G., et al. (2002) An ectopic mediastinal parathyroid adenoma accurately located by a single-day imaging protocol of tc-99m pertechnetate-mibi subtraction scintigraphy and mibi-spect-computed tomographic image fusion. *Clin. Nucl. Med. 27*, 186−190.
(4) Chance, B., Kang, K., He, L., Weng, J., and Sevick, E. (1993) Highly sensitive object location in tissue models with linear in-phase and antiphase multielement optical arrays in one and 2 dimensions. *Proc. Natl. Acad. Sci. U.S.A. 90*, 3423−3427.
(5) Ntziachristos, V., and Weissleder, R. (2001) Experimental three-dimensional fluorescence reconstruction of diffuse media by use of a normalized born approximation. *Opt. Lett. 26*, 893−895.
(6) Graves, E. E., Ripoll, J., Weissleder, R., and Ntziachristos, V. (2003) A submillimeter resolution fluorescence molecular imaging system for small animal imaging. *Med. Phys. 30*, 901−911.
(7) Patwardhan, S. V., Bloch, S. R., Achilefu, S., and Culver, J. P. (2005) Time-dependent whole-body fluorescence tomography of probe bio-distributions in mice. *Opt. Express 13*, 2564−2577.
(8) Ntziachristos, V., Ripoll, J., Wang, L. H. V., and Weissleder, R. (2005) Looking and listening to light: The evolution of whole-body photonic imaging. *Nat. Biotechnol. 23*, 313−320.
(9) Ntziachristos, V., Yodh, A. G., Schnall, M., and Chance, B. (2000) Concurrent mri and diffuse optical tomography of breast after indocyanine green enhancement. *Proc. Natl. Acad. Sci. U.S.A. 97*, 2767−2772.
(10) Torchilin, V. P. (2002) Peg-based micelles as carriers of contrast agents for different imaging modalities. *Adv. Drug Delivery Rev. 54*, 235−252.
(11) Trubetskoy, V. S. (1999) Polymeric micelles as carriers of diagnostic agents. *Adv. Drug Delivery Rev. 37*, 81−88.
(12) Josephson, L., Kircher, M. F., Mahmood, U., Tang, Y., and Weissleder, R. (2002) Near-infrared fluorescent nanoparticles as combined mr/optical imaging probes. *Bioconjugate Chem. 13*, 554−560.
(13) Modo, M., Cash, D., Williams, S. C. R., Mellodew, K., and Price, J., et al. (2004) Mapping transplanted stem cell migration after a stroke: A serial, in vivo magnetic resonance imaging study. *Neuroimage 21*, 311−317.
(14) Ballou, B., Fisher, G. W., Hakala, T. R., and Farkas, D. L. (1997) Tumor detection and visualization using cyanine fluorochrome- labeled antibodies. *Biotechnol. Prog. 13*, 649−658.
(15) Manning, H. C., Bornhop, D. J., Goebel, T., Thompson, R. C., and Price, R. R., et al. (2004) Targeted molecular imaging agents for cellular-scale bimodal imaging. *Bioconjugate Chem. 15*, 1488−1495.
(16) Zhang, Z., and Achilefu, S. (2004) Synthesis and evaluation of polyhydroxylated near-infrared carbocyanine molecular probes. *Org. Lett. 6*, 2067−2070.
(17) Atherton, E., and Sheppard, R. C. (1989) Solid-phase peptide synthesis: A practical approach. In *Practical Approach Series* (Rickwood, D., and Hames, B. D., Eds.) Oxford University Press, Oxford, England.
(18) Achilefu, S., Jimenez, H. N., Dorshow, R. B., Bugaj, J. E., and Webb, E. G., et al. (2002) Synthesis, in vitro receptor binding, and in vivo evaluation of fluorescein and carbocyanine peptide-based optical contrast agents. *J. Med. Chem. 45*, 2003−2015.
(19) Achilefu, S., Dorshow, R. B., Bugaj, J. E., and Rajagopalan, R. (2000) Novel receptor-targeted fluorescent contrast agents for in vivo tumor imaging. *Invest. Radiol. 35*, 479−485.
(20) Hawrysz, D. J., and Sevick-Muraca, E. M. (2000) Developments toward diagnostic breast cancer imaging using near-infrared optical measurements and fluorescent contrast agents. *Neoplasia 2*, 388−417.
(21) Achilefu, S. (2004) Lighting up tumors with receptor-specific optical molecular probes. *Technol. Cancer Res. Treat. 3*, 393−409.
(22) Geddes, C. D., Cao, H., Gryczynski, I., Gryczynski, Z., and Fang, J. Y., et al. (2003) Metal-enhanced fluorescence (mef) due to silver colloids on a planar surface: Potential applications of indocyanine green to in vivo imaging. *J. Phys. Chem. A 107*, 3443−3449.
(23) Tarazi, L., George, A., Patonay, G., and Strekowski, L. (1998) Spectral characterization of a novel near-infrared cyanine dye: A study of its complexation with metal ions. *Talanta 46*, 1413−1424.
(24) Higuchi, T., Yang, D. J., Ilgan, S., Tansey, L. W., and Zareneyrizi, F., et al. (1999) Biodistribution and scintigraphy of in-111 dtpa-adriamycin in mammary tumor-bearing rats. *Anti-Cancer Drugs 10*, 89−95.
(25) Swailem, F. M., and Shah, J. (1998) In-vivo tissue uptake and retention of sn-117m(4+)dtpa in a human subject with metastatic bone pain and in normal mice (vol 25, pg 279, 1998). *Nucl. Med. Biol. 25*, 515−515.

BC050136S